land

Article

A Green Infrastructure Prioritization Index Combining Woody Vegetation Deficits and Social Vulnerability in Temuco, Chile

Germán Catalán [1,2], Carlos Di Bella [3,4], Camilo Matus-Olivares [5], Paula Meli [6,7], Francisco De La Barrera [8,9], Rosa Reyes-Riveros [2,10], Rodrigo Vargas-Gaete [11,12], Sonia Reyes-Packe [13] and Adison Altamirano [2,*]

1 Doctorado en Ciencias Agroalimentarias y Medioambiente, Universidad de La Frontera, Temuco 4811230, Chile; german.catalan@ufrontera.cl
2 Laboratorio de Ecología del Paisaje y Conservación, Universidad de La Frontera, Temuco 4811230, Chile; rreyes@uct.cl
3 Instituto de Investigaciones Fisiológicas y Ecológicas Vinculadas a la Agricultura (IFEVA), Facultad de Agronomía, Universidad de Buenos Aires, CONICET, Buenos Aires C1417, Argentina; dibellac@agro.uba.ar
4 Departamento de Métodos Cuantitativos y Sistemas de Información, Facultad de Agronomía, Universidad de Buenos Aires, Av. San Martín 4453, Buenos Aires C1417, Argentina
5 Complex Engineering System Institute—ISCI, Santiago 8370076, Chile; camilo.matus@ufrontera.cl
6 Natura y Ecosistemas Mexicanos, A.C., Ciudad de México 01000, Mexico; paula@naturamexicana.org
7 Fundación Internacional para la Restauración de Ecosistemas—Argentina, Colón 3280, Argentina
8 Centro de Desarrollo Urbano Sustentable (CEDEUS), Concepción 3349001, Chile; fdelabarrera@udec.cl
9 Facultad de Ciencias Ambientales, Universidad de Concepción, Concepción 3349001, Chile
10 Departamento de Ciencias Ambientales, Facultad de Recursos Naturales, Universidad Católica de Temuco, Rudecindo Ortega 2950, Temuco 4811230, Chile
11 Laboratorio de Ecosistemas y Bosques (EcoBos), Departamento de Ciencias Forestales, Universidad de La Frontera, Casilla 54-D, Francisco Salazar 01145, Temuco 4811230, Chile; rodrigo.vargas@ufrontera.cl
12 Centro Nacional de Excelencia para la Industria de la Madera (CENAMAD), Pontificia Universidad Católica de Chile, Vicuña Mackenna 4680, Santiago 6904411, Chile
13 Facultad de Agronomía y Sistemas Naturales, Pontificia Universidad Católica de Chile, Vicuña Mackenna 4680, Santiago 6904411, Chile; sonia.reyes@uc.cl
* Correspondence: adison.altamirano@ufrontera.cl

Abstract

This study developed and tested a neighborhood-scale framework that integrates unmanned aerial vehicle (UAV)-based multispectral mapping and georeferenced socioeconomic data to identify inequities in urban green infrastructure and translate them into an operational prioritization tool for inclusive planning. Using object-based image analysis, impervious surfaces, low vegetation, and woody vegetation (trees and shrubs) were mapped across 33 Neighborhood Units in Temuco, Chile, and landscape metrics describing dominance, edge, isolation/connectivity, and diversity were derived. Socioeconomic conditions were summarized through Principal Component Analysis, and their relationships with vegetation metrics were evaluated using Generalized Additive Models. The results revealed strongly nonlinear and metric-specific associations, with the most robust relationships observed for woody-structure metrics, particularly total woody edge and built-environment isolation, whereas landscape diversity showed weaker but still significant dependence on resource-access gradients. To support inclusive planning, a dimensionless Green Infrastructure Prioritization Index (GIPI) was computed by combining standardized green deficit and standardized social vulnerability with equal weights. GIPI values ranged from 0.318 to 0.740 (median = 0.528), identifying 11 high-priority units characterized by higher social vulnerability and less favorable woody structure, including lower largest-patch dominance and greater isolation. Sensitivity analyses varying the deficit weight from 0.30 to 0.70 showed that 10 of the 11 high-priority units remained in the same class in at least 80% of weighting scenarios, indicating a stable priority set. Further classification of high-priority units according to dominant deficit type supported a staged

Academic Editor: Thomas Panagopoulos

Received: 12 February 2026
Revised: 21 March 2026
Accepted: 27 March 2026
Published: 31 March 2026

intervention strategy, in which woody canopy is first increased in deficit nodes and subsequently reinforced through corridor-oriented greening to improve structural connectivity. These findings demonstrate the value of coupling fine-scale vegetation mapping with socioeconomic gradients to support more equitable urban green infrastructure planning.

Keywords: UAV; urban vegetation; landscape metrics; environmental justice; urban planning; object-based image analysis; Chile

1. Introduction

Rapid urban growth across cities of the Global South, including many intermediate cities, has intensified sociospatial inequalities in access to and quality of green infrastructure, with important implications for human well-being, urban climate regulation, and biodiversity conservation [1–4]. Although the benefits of urban vegetation are widely recognized, empirical evidence indicates that these benefits are unevenly distributed within cities and often favor socioeconomically advantaged areas, although the magnitude and direction of these patterns may vary according to regional context and spatial scale [2,3,5,6]. In this context, a critical gap persists between the biophysical assessment of urban vegetation and the development of operational planning tools capable of prioritizing interventions from an equity-oriented perspective [1,7].

Cities concentrate people, infrastructure, and opportunity, but also climate risk and health burdens. As the urban share of the global population continues to rise, the capacity of cities to deliver basic environmental conditions that support well-being has become a central sustainability challenge [8]. Urban vegetation and public green spaces are among the most policy-relevant urban nature assets because they provide multiple, measurable co-benefits and ecosystem services, including microclimate regulation, thermal comfort, air-quality improvement, habitat support, risk reduction, and health-supporting environments across the life course [9–12]. These benefits have been codified in global agendas that treat access to public space as a development target (e.g., Sustainable Development Goals [SDG] 11.7.1), reinforcing the need for tractable, spatially explicit indicators that can be evaluated at the intra-urban scale where inequalities are produced and experienced [13,14]. However, urban greening is not experienced uniformly. A consistent finding across the scientific literature is that green infrastructure and tree canopy tend to be unevenly distributed, often aligning with socioeconomic gradients in ways that compound vulnerability to heat and other hazards [15]. This "double burden" matters because the places with the greatest need for climate buffering and restorative environments are frequently those with the least access to high-quality, well-connected urban nature. At the same time, greening initiatives can generate unintended distributive effects through "green gentrification" if implementation is not paired with equity safeguards and community-centered governance [16]. Together, these lines of evidence imply that urban vegetation assessments should move beyond citywide averages to identify actionable gaps at neighborhood scales, while explicitly linking biophysical deficits to equity-oriented decision rules.

Most previous studies rely on aggregated green coverage metrics, which limits understanding of how vegetation structure and spatial configuration, particularly woody vegetation, shape key ecosystem functions such as shade provision, ecological connectivity, and urban heat mitigation [11,12,17]. Moreover, planning-oriented approaches often lack explicit mechanisms to integrate high-resolution spatial information with socioeconomic indicators, constraining the identification of priority units that jointly exhibit ecological deficits and social vulnerability [18,19]. This limitation is especially pronounced in Global

South cities, where rapid urban expansion and socio-spatial inequality unfold simultaneously. A recent synthesis of high- and very-high-resolution remote sensing for urban vegetation concluded that very-high-resolution (VHR) approaches substantially broaden the analytical scope of intra-urban greenness assessment by enabling object-level characterization and policy-relevant indicators, while also documenting persistent gaps in equity-oriented applications, particularly across underrepresented urban contexts [20]. Unmanned aerial vehicles (UAVs), in particular, provide centimeter-scale multispectral products and surface models that are well suited to heterogeneous urban environments, where vegetation is interwoven with narrow streets, small parcels, and mixed land uses [21,22].

A second barrier is analytical rather than observational: socio-environmental relationships within cities are frequently nonlinear and threshold-driven, so purely linear models may obscure inflection points where small changes in socioeconomic conditions coincide with abrupt shifts in vegetation amount or configuration. Generalized Additive Models (GAMs) are widely used for this purpose because they estimate flexible smooth functions while retaining interpretability, making them appropriate for identifying neighborhood-scale nonlinearities that can inform targeting and sequencing of interventions [23,24]. Dimensionality reduction techniques, such as Principal Component Analysis (PCA), complement this approach by consolidating collinear socioeconomic indicators into a small set of interpretable axes suitable for neighborhood comparisons and index construction [25,26].

This study adopts a functional rather than purely demographic definition of intermediate cities, understanding them as urban centers defined less by a fixed demographic threshold than by the position and functions they occupy within regional and national urban systems, acting as interface nodes between metropolitan areas, smaller settlements, and their surrounding territories [27,28]. Although they are smaller than major metropolitan centers, these cities frequently undergo rapid and sometimes poorly controlled expansion, display heterogeneous urbanization trajectories, and reproduce persistent socio-spatial inequalities [7,27,29]. At the same time, they remain comparatively underrepresented in the scientific literature on urban systems, while the evidence base on urban nature and ecosystem services is still disproportionately concentrated in larger cities and a limited set of contexts; in parallel, research on green infrastructure justice is still expanding its empirical and conceptual scope [15,30,31].

Taken together, the literature reveals three interrelated gaps: the underrepresentation of intermediate Global South cities in high-resolution urban greenness research; the limited analytical attention paid to vegetation spatial configuration, particularly fragmentation and connectivity; and the lack of integrated frameworks that combine fine-scale biophysical data, socioeconomic vulnerability, and decision-oriented prioritization for equity-focused planning.

Against this background, the general objective of this study is to develop and apply an integrated neighborhood-scale framework that combines UAV-based multispectral remote sensing with georeferenced socioeconomic data to analyze urban vegetation from both biophysical and social perspectives in a mid-sized Latin American city. Specifically, the study aims to: (i) characterize the spatial configuration of urban vegetation, with emphasis on fragmentation and connectivity; (ii) assess how these vegetation patterns relate to neighborhood-level socioeconomic conditions; and (iii) translate these findings into an equity-oriented prioritization approach to support more inclusive and spatially explicit urban planning. By moving beyond vegetation amount alone, the proposed framework provides a more policy-relevant understanding of urban green infrastructure and its uneven distribution across the urban landscape.

2. Materials and Methods

2.1. Study Area

The study area comprises the urban zone of Temuco (38°44′ S, 72°35′ W), capital of the Araucanía Region in southern Chile (Figure 1). Located at an altitude of approximately

120 m above sea level, the city covers an area of around 3000 hectares. The climate is temperate oceanic with a Mediterranean influence (Csb/Cfb according to Köppen classification), characterized by dry summers and rainy winters, which dictates the distinct seasonality of the urban vegetation. As an intermediate-sized city, Temuco presents a heterogeneous urban fabric shaped by rapid expansion and a significant Mapuche indigenous population, creating a diverse socio-spatial mosaic ideal for analyzing the interplay between socioeconomic gradients and vegetation structure.

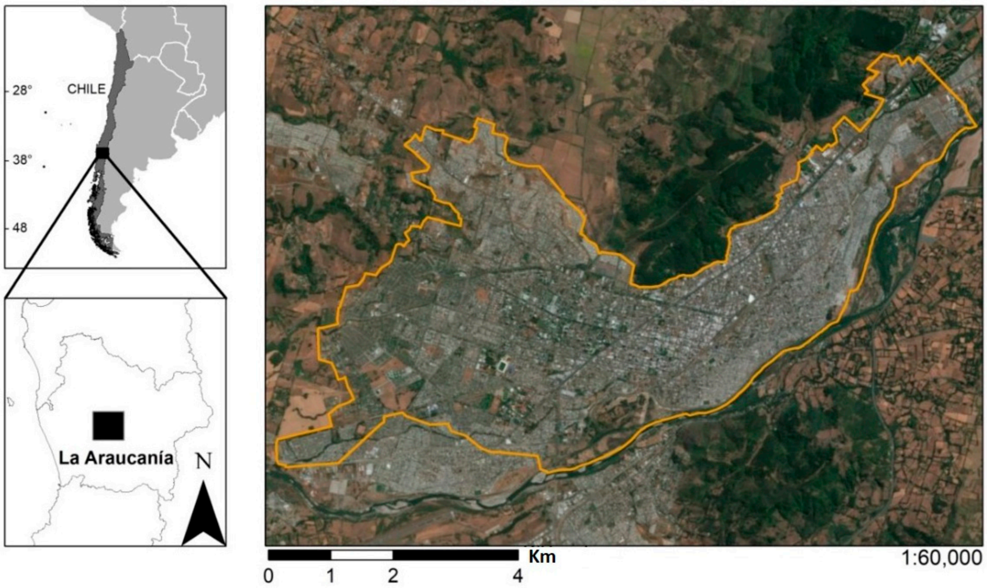

Figure 1. Study area. The region enclosed in orange represents the effective study area; adjacent urban sectors were omitted due to DGAC (Civil Aviation Authority) safety restrictions for flights near airport zones.

The methodology of this work is summarized in Figure 2, after which the details of each of the aspects addressed are presented.

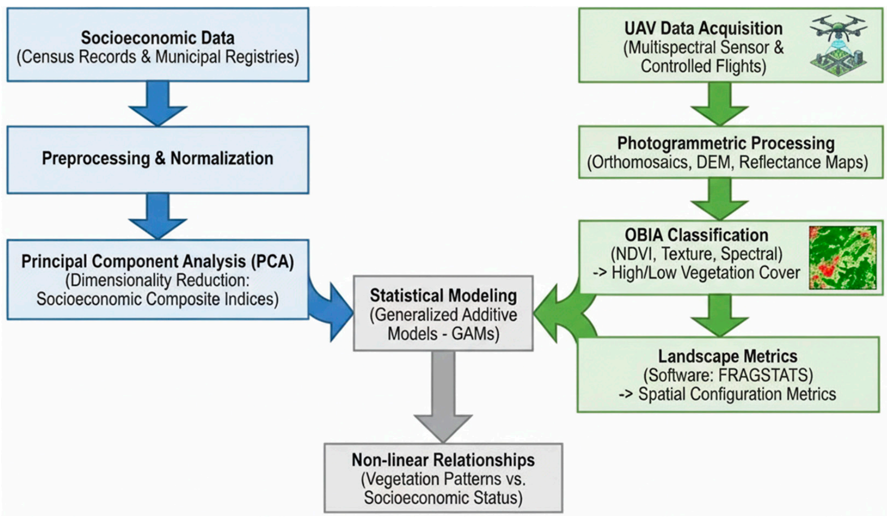

Figure 2. Methodological workflow of the study. The flowchart illustrates the integration of two primary data streams: socioeconomic indicators (**left**) and high-resolution UAV imagery (**right**). Socioeconomic data were standardized and reduced using Principal Component Analysis (PCA). UAV imagery underwent photogrammetric processing and Object-Based Image Analysis (OBIA) to classify vegetation into structural categories. Landscape metrics were computed using FRAGSTATS to quantify spatial configuration. Finally, both data streams were integrated using Generalized Additive Models (GAMs) to detect non-linear relationships.

2.2. Acquisition and Processing of Aerial Imagery

A DJI Phantom IV unmanned aerial vehicle (DJI, Shenzhen, China) equipped with a Parrot Sequoia multispectral camera (Parrot, Paris, France) and a Mars P4 Lite emergency parachute system (MARS, Jevíčko, Czech Republic) was used for aerial data acquisition, ensuring both high imaging precision and operational safety during flight missions. The Parrot Sequoia sensor simultaneously captures RGB imagery and four narrow spectral bands—green (550 nm ± 40 nm), red (660 nm ± 40 nm), red-edge (735 nm ± 10 nm), and near-infrared (790 nm ± 40 nm)—which are well-suited for vegetation and canopy reflectance analysis in urban environments.

Data collection was conducted between 12:00 and 16:00 local time under clear, stable atmospheric conditions during January and February 2018, to minimize illumination variability and shadow effects associated with low solar angles. A total of 102 flight missions were performed, each covering approximately 40–50 ha, with an average flight duration of about 20 min. Flight paths were preprogrammed using DroneDeploy (DroneDeploy, San Francisco, CA, USA; available online: https://www.dronedeploy.com; accessed on 12 February 2018) to ensure consistent coverage and data quality, maintaining a flight altitude of 200 m above ground level and an image overlap of 75% in both the front and side directions. These settings resulted in a ground sampling distance (GSD) of approximately 7 cm per pixel for RGB imagery and 20 cm per pixel for multispectral data (NIR and Red Edge spectral bands), providing spatial detail sufficient for fine-scale vegetation and land-cover mapping.

To standardize image acquisition, the Parrot Sequoia multispectral camera used its integrated sunshine sensor, which continuously measures incoming solar irradiance across the same spectral bands captured by the camera. These irradiance data were used to compensate for illumination variability during each flight, thereby improving radiometric consistency across missions. In addition, a calibrated reflectance panel supplied by the manufacturer was used before and after each flight to normalize surface reflectance values and support radiometric calibration.

Both RGB and multispectral datasets were automatically geotagged using positional information from the UAV's onboard Global Navigation Satellite System (GNSS) and the camera's internal GPS. All imagery was processed in Pix4D Mapper v.4.6.3 (Pix4D S.A. Prilly, Switzerland) following a standardized photogrammetric workflow. First, radiometric calibration was applied to the multispectral imagery using the sunshine sensor and calibrated reflectance panel. Orthomosaics were then generated for RGB imagery and for each multispectral band (green, red, red-edge, and near-infrared).

Derived products included a Digital Surface Model (DSM), a Digital Terrain Model (DTM), and reflectance maps for each spectral band. Pix4D Mapper automatically applied the geometric and radiometric corrections required for orthomosaic generation [32]. The final outputs achieved spatial resolutions of approximately 7 cm pixel^{-1} for RGB imagery and 20 cm pixel^{-1} for multispectral imagery. The resulting 102 orthomosaics were subsequently merged into a single composite mosaic to enable a spatially continuous analysis of vegetation patterns across the study area.

2.3. Vegetation Classification

An Object-Based Image Analysis (OBIA) approach was implemented in eCognition Developer v.9.3 (Trimble, Munich, Germany) to classify vegetation into two structural categories: woody vegetation (trees and shrubs) and low vegetation (grasses and herbaceous cover). OBIA was selected because it integrates spectral, spatial, and contextual information, thereby improving the accuracy of urban vegetation classification compared with traditional pixel-based methods, which often suffer from spectral confusion in heterogeneous urban environments [32–35].

Image segmentation was performed using the Multiresolution Segmentation (MRS) algorithm, which aggregates adjacent pixels with similar spectral and spatial characteristics into meaningful image objects. This algorithm optimizes homogeneity criteria based on three user-defined parameters: scale, shape, and compactness, which together control the size and geometry of resulting segments [36,37]. In this study, the parameters were set to a scale of 5, a shape factor of 0.1, and a compactness value of 0.5, providing a balance between boundary precision and internal homogeneity. These settings allowed for detailed delineation of vegetation patches while minimizing over-segmentation, consistent with previous applications in high-resolution urban vegetation mapping [38–42].

Vegetation objects were identified using the Normalized Difference Vegetation Index (NDVI), calculated from the near-infrared (NIR) and red bands according to the standard formulation proposed by Rouse et al. [43]:

$$NDVI = \frac{NIR - Red}{NIR + Red} \tag{1}$$

where NIR and R are the near-infrared and red reflectances, respectively.

NDVI enhances the contrast between vegetated and non-vegetated surfaces because healthy vegetation typically exhibits high reflectance in the near-infrared and strong absorption in the red region of the spectrum [44–46]. Additional thresholds in the visible RGB bands were used to exclude shadows and other non-vegetated features [47,48].

To distinguish woody from low-stature vegetation, the NDVI-derived vegetation mask was integrated with a normalized Digital Surface Model (nDSM), calculated as the difference between the Digital Surface Model (DSM) and the Digital Terrain Model (DTM) (nDSM = DSM − DTM). This height-normalized product enabled the joint use of spectral and structural information by isolating above-ground object height [5–8]. Vegetation objects with a mean nDSM height > 0.5 m were classified as woody vegetation (primarily trees and shrubs), whereas those with a mean height $\leq$ 0.5 m were assigned to the low-vegetation category (mainly grasses and herbaceous cover) [47,49]. Integrating spectral indices with height-normalized elevation data improves classification robustness in heterogeneous urban environments, where shadows, built structures, and surface reflectance variability may otherwise generate spectral ambiguities [47,50,51].

Classification accuracy was assessed using 300 stratified random validation points distributed across the study area and allocated among the evaluated land-cover classes. The class assigned to each point was independently verified through visual interpretation of high-resolution RGB imagery in order to ensure an unbiased evaluation of the classification results. Based on these reference data, a confusion matrix was generated to quantify classification performance by comparing the mapped classes with the observed classes at each validation point. From this matrix, two widely used accuracy metrics were calculated: Overall Accuracy (OA), which represents the proportion of correctly classified samples relative to the total number of validation samples, and the Kappa Coefficient (κ), which measures the degree of agreement between the classification and the reference data while accounting for agreement expected by chance [52,53]. The full confusion matrix is provided in Table S1 of the Supplementary Material.

2.4. Landscape Metrics Calculation

To characterize the spatial configuration of vegetation and the built environment at the neighborhood level, FRAGSTATS v.4.2 [54] was employed. The analysis focused on a curated set of landscape metrics (detailed in Table 1) selected to capture four distinct ecological dimensions relevant to urban planning: (i) diversity, to assess landscape heterogeneity;

(ii) dominance, to measure the continuity of cover types; (iii) isolation, to quantify physical connectivity between patches; and (iv) shape complexity, to evaluate the irregularity of the spatial fabric. This multidimensional approach provides a robust quantitative framework to assess the structural integrity of vegetation patterns and their implications for urban equity.

Table 1. Summary of landscape metrics selected to quantify the spatial structure of vegetation and the built environment in Temuco.

Functional Category	Acronym	Metric Name	Description and Ecological Interpretation	Key References
Diversity	SHDI	Shannon's Diversity Index	Quantifies the diversity of patch types within the landscape, considering both abundance and evenness. In urban contexts, a higher value indicates a heterogeneous landscape with multiple cover classes (e.g., trees, grass, built-up areas), often associated with higher richness of ecosystem services.	[54–57]
Dominance/Area	LPI	Largest Patch Index	Percentage of the landscape occupied by the largest patch of a specific class. It serves as a dominance indicator. A high LPI in built-up classes implies continuous soil sealing, while in vegetation classes, it suggests consolidated habitat cores.	[56,58–60]
Isolation/ Connectivity	ENN_MN	Mean Euclidean Nearest Neighbor Distance	Average of the shortest straight-line distances (edge-to-edge) between a patch and its nearest neighbor of the same class. It is a critical proxy for isolation. Higher values indicate greater fragmentation and lower ecological connectivity, hindering biological flows and human access.	[54,57].
Shape/ Complexity	PAFRAC	Perimeter–Area Fractal Dimension	Evaluates patch shape complexity based on the perimeter–area relationship (range 1–2). Values near 1 indicate simple, geometric shapes (typical of anthropic/planned structures), while values near 2 indicate complex, irregular shapes (natural features). Useful for distinguishing planned vs. informal urbanization patterns.	[61–63]

2.5. Socioeconomic Data Collection and Preprocessing

This research integrated a selected set of socioeconomic variables to gain a comprehensive understanding of demographic, housing, and service-related aspects in each Neighborhood Unit. The following indicators were considered: population characteristics (total population, gender distribution, age brackets, number of migrants, and individuals identifying as part of an indigenous community), housing characteristics (total number of private, collective, and occupied housing units; building type; predominant wall and roof materials; floor composition; and source of water supply), and urban services (specifically restricted to the availability of educational facilities and healthcare services). Data were obtained from the public platform Dato Vecino [64], which centralizes statistical information at the municipal and regional levels in Chile. Priority was given to indicators with the most recent temporal coverage to ensure relevance and data reliability. The information was compiled in a structured tabular format (CSV), and subsequent preprocessing and quality validation were conducted by reviewing metadata, variable definitions, and potential anomalies, including outliers and duplicate records. Each dataset was then integrated into a central repository, recording the date of access and any specific data attributes. This systematization facilitated the application of statistical techniques and visualization tools for identifying relevant spatial patterns and trends, thus creating a robust foundation to correlate socioeconomic information with vegetation classification outputs and landscape metrics [65,66].

2.6. Data Preprocessing and Variable Selection

Prior to statistical modeling with the Generalized Additive Models (GAMs) described in Section 2.7, a rigorous data preprocessing strategy was applied to define the predictor and response variables. This step was essential to address the high dimensionality and multicollinearity inherent in both the socioeconomic and landscape metric datasets, ensuring robust inputs for the models.

For the socioeconomic predictors, multicollinearity was severe and pervasive across the 22 original variables described in Supplementary Table S2 (e.g., strong correlations between population size and housing quality). To address this issue without discarding information, and to mitigate the high risk of overfitting caused by the excess of predictors relative to the limited number of observations ($N = 33$), Principal Component Analysis (PCA) was applied to the standardized dataset. The first four principal components (PC1–PC4), which cumulatively explained 83.9% of the total variance, were retained as orthogonal predictors for the GAM analysis.

For the vegetation response variables, a correlation analysis (Pearson's $|r| \geq 0.6$) revealed distinct clusters of redundancy. For instance, 13 metrics related to diversity and fragmentation were highly correlated; thus, Shannon's Diversity Index (SHDI) was selected as the representative metric for this cluster due to its ecological comprehensiveness. Similarly, Total Edge of Woody vegetation was selected to represent the structural boundary cluster. Six other metrics showed low correlations and were retained as independent response variables. This selection process resulted in a final set of eight distinct vegetation metrics to be modeled separately, which are summarized in Figure S2 and drawn from the full set of calculated metrics reported in Supplementary Table S3.

2.7. Statistical Modeling with Generalized Additive Models

To evaluate the relationships between the socioeconomic gradients and the spatial configuration of vegetation, Generalized Additive Models (GAMs) were employed. Unlike traditional linear regression, GAMs provide a flexible framework that models the relationship between predictors and the response variable through smooth functions rather than rigid linear coefficients. This approach allows the data to determine the shape of the curve, enabling the detection of complex non-linear patterns such as thresholds or saturation points.

In this study, separate GAMs were fitted for each of the eight selected landscape metrics (response variables). The four socioeconomic principal components (PC1–PC4) served as the independent predictors in all models. Penalized cubic splines were utilized as the smoothing basis to estimate the non-linear effects. To ensure model robustness and prevent overfitting—a key consideration given the sample size ($N = 33$)—the degree of smoothness for each term was automatically optimized using Generalized Cross-Validation (GCV), which balances model complexity with explanatory power.

2.8. Operationalization of Inclusive Strategies and Prioritization

2.8.1. Social Vulnerability Score (V): Construction from Neighborhood Indicators

Because no single neighborhood-level vulnerability index was available, a composite vulnerability score was constructed from census-derived indicators and used as the vulnerability component in the GIPI. Vulnerability was operationalized using rates capturing (i) housing precarity (shares of dwellings with precarious wall materials, poor roof quality, and poor floor quality), (ii) basic infrastructure deficit (share of households relying on non-public water sources), (iii) service deficits (inverse of education and healthcare facilities per 10,000 inhabitants), and (iv) demographic sensitivity (share of population aged 65+). Population density (inhabitants per hectare) was additionally included to capture overcrowding pressures at the neighborhood scale. All components were standardized using z-scores and aggregated additively with equal weights to produce a standardized vulnerability score V_Z. For integration into the prioritization framework, V_Z was min–max normalized to [0, 1], yielding V.

2.8.2. Green Deficit Score (G_{def}): Standardization, Directionality, and Aggregation

A green deficit score was computed to summarize the biophysical lack of green infrastructure in each neighborhood unit. Inputs included: (i) vegetated proportion deficit, computed as $1 - \text{PROPVEG}$, and (ii) landscape configuration metrics characterizing fragmentation and disconnection of the vegetated class (e.g., mean nearest-neighbor distance and edge density), together with a dominance metric (largest patch index), where higher values indicate better conditions.

Each input was standardized (z-scores). Variables where higher values indicate better conditions (e.g., dominance metrics such as LPI) were inverted so that higher standardized values consistently represent greater deficit. The composite green deficit score was then calculated as the mean of standardized deficit indicators:

$$G_{def} = \frac{1}{k}\sum_{j=1}^{k} z_{j,\text{def}} \tag{2}$$

Finally, G_{def} was normalized to [0, 1] for combination with V.

2.8.3. Green Infrastructure Prioritization Index (GIPI) and Sensitivity Analysis

The Green Infrastructure Prioritization Index (GIPI) was computed as a weighted combination of normalized green deficit and social vulnerability:

$$GIPI = w_g G_{def} + w_v V, \quad w_g + w_v = 1 \tag{3}$$

Equal weights were used as the default ($w_g = w_v = 0.5$). To evaluate robustness, a weight sensitivity analysis was performed a weight sensitivity analysis by varying w_g from 0.30 to 0.70 (step = 0.05), recalculating GIPI and neighborhood priority categories (terciles: Low/Medium/High) under each configuration. Stability was assessed by agreement in priority classes and rank-order consistency relative to the default weighting.

3. Results

3.1. Land Cover Composition Across Neighborhood Units

The acquisition and processing of high-resolution UAV imagery enabled a detailed classification of land cover types across the studied neighborhood units. To characterize the significant spatial variability inherent to the urban fabric of Temuco, descriptive statistics were calculated for each cover class. Table 2 summarizes the distribution of non-vegetated (impervious) and vegetated surfaces, presenting median values and observed ranges (minimum and maximum) for the "non-vegetated", "low vegetation", and "woody vegetation" classes. These aggregated metrics highlight the substantial heterogeneity in green infrastructure provision across the city.

Table 2. Descriptive statistics of land cover classes obtained via UAV-based OBIA classification in Temuco's neighborhood units.

Land Cover Class	Description	Median Coverage (%)	Observed Range (Min–Max) (%)
Non-Vegetated (Impervious)	Includes buildings, pavements, streets, and bare soil.	79.3	68.3–96.4
Woody Vegetation (Tree/Shrub)	Trees and shrubs with height > 0.5 m.	5.6	0.8–17.6
Low Vegetation (Herbaceous)	Grass and herbaceous cover < 0.5 m.	14.6	2.8–23.2
Total Vegetation	Sum of high and low vegetation classes.	20.7	3.6–31.7

The quantitative analysis of land cover composition indicates substantial heterogeneity across the study area. The neighborhood unit 5 de Abril (143.81 ha) exhibited 75.50% impervious cover, with the remaining area distributed between low vegetation (14.60%) and woody vegetation (9.90%). In contrast, José Miguel Carrera (339.95 ha) presented a lower proportion of non-vegetated surfaces (68.30%) and a combined vegetation coverage of 31.70%. Regarding the extremes of the distribution, Tromen, the largest unit analyzed (347.05 ha), recorded 80.20% non-vegetated cover and 19.80% total vegetation. Conversely, Los Laureles (13.27 ha) presented the lowest vegetation coverage values, with only 11.90% (1.58 ha) of its total area classified as green space.

3.2. Spatial Patterns of Landscape Metrics

Following the classification, landscape metrics computed via FRAGSTATS quantified the spatial structure across the analyzed neighborhoods. The Largest Patch Index (LPI) for impervious surfaces yielded a maximum of 96.17% in the 'Central' unit, indicating a highly consolidated built environment, compared to 81.17% in 'Balmaceda'. In terms of composition, Shannon's Diversity Index (SHDI) recorded values exceeding 0.80 in 'Imperial' and 'Igualdad y Trabajo', indicating the highest proportional evenness among cover classes in the study area.

Regarding spatial configuration, the Mean Nearest Neighbor Distance (ENN_MN) for vegetation classes presented higher values in neighborhoods such as 'Paredes' and 'Ernesto Bohn' relative to the sample median, denoting greater patch isolation. Finally, shape complexity metrics for low vegetation showed Edge Density (ED) values ranging from approximately 315 to 2000 m/ha, alongside higher Fractal Dimension (PAFRAC) scores compared to the "non-vegetated" class, denoting greater boundary irregularity in herbaceous patches.

3.3. Socioeconomic Data

The socioeconomic dataset revealed substantial demographic and infrastructural variability across the analyzed neighborhood units. Total population ranged from a minimum of 716 inhabitants in 'Central' to a maximum of 28,238 in 'Tromen'. Regarding housing materiality, the presence of precarious construction materials (e.g., waste or improvised materials for walls and roofs) was highest in units such as 'Paredes', 'Millaray', and 'José Miguel Carrera'. In terms of utility infrastructure, while the majority of neighborhoods reported high connection rates to the public water grid, specific peripheral zones recorded a dependence on non-networked water sources. Furthermore, the spatial distribution of institutional services showed a concentration of educational and healthcare facilities in established districts, with lower density counts recorded in peri-urban units.

https://doi.org/10.3390/land15040574

3.4. Characterization of Socioeconomic Gradients

Principal Component Analysis retained four components (PC1 to PC4) that cumulatively explain 83.9% of the total variance in the socioeconomic dataset. The first component (PC1), accounting for 52.8% of the variance, constitutes the dominant axis of socio-housing differentiation in the city (see Figure S1 and Table S2 of the Supplementary Material). This component is defined by high positive loadings for total population density and variables associated with precarious housing materiality, specifically the quality of roofs and floors. Consequently, this axis orders neighborhood units along a gradient ranging from low-density areas with consolidated housing to densely populated zones exhibiting significant qualitative deficits in housing infrastructure. The second component (PC2), represents a demographic and cultural gradient that operates independently of housing quality (see Figure S1 of the Supplementary Material). This axis is characterized by a strong positive association with the proportion of indigenous population and gender structure, capturing spatial distribution patterns of Mapuche communities that are not necessarily collinear with material precariousness. Finally, the remaining components capture dimensions of specific services and infrastructure (see Figure S1 of the Supplementary Material). PC3 (10.8% of variance) defines access to institutional services, showing dominant loadings for the number of educational and healthcare facilities available. PC4 (5.9% of variance) identifies a residual gradient of resources and basic infrastructure, determined primarily by the reliance on water sources other than the public network and the presence of an older adult population.

3.5. Variable Selection and Spatial Configuration of Vegetation

The redundancy analysis of the 23 calculated landscape metrics revealed distinct patterns of collinearity, identifying two dominant clusters of information (see Figure S2 of the Supplementary Material). The first cluster, associated with general Diversity and Fragmentation, showed strong correlations among 13 metrics; consequently, Shannon's Diversity Index (SHDI) was selected as the representative variable for this group due to its ecological comprehensiveness. The second cluster, related to Edge and Density, was effectively summarized by the Total Tree Edge. Six additional metrics, including shape complexity (PAFRAC) and patch dominance (LPI), were identified as statistically independent dimensions and were retained for separate modeling.

Descriptive statistics for the full set of calculated landscape metrics are presented in Table S3, while the subset retained for modeling is identified in Figure S2. These results reveal a highly heterogeneous urban fabric. SHDI exhibited substantial variability across the 33 neighborhood units, indicating that while some areas maintain a diverse mosaic of vegetation classes, others are dominated by homogeneous land covers. Regarding the arboreal structure, showed marked contrasts, suggesting that trees are not uniformly distributed but rather clustered in specific zones, creating distinct gradients of green infrastructure availability. This selection of non-redundant metrics confirms that the physical arrangement of green spaces (shape and isolation) varies independently of their diversity or total edge, reinforcing the need to analyze them as distinct ecological dimensions.

3.6. Associations Between Socioeconomic Gradients and Vegetation

The application of GAMs revealed distinct and significant associations between the socioeconomic gradients and the spatial configuration of urban vegetation (Figure 3). A detailed statistical summary of all eight models, including goodness-of-fit metrics and parameters for non-significant predictors, is provided in Supplementary Table S4. The explanatory power of the models varied considerably depending on the landscape metric analyzed, indicating that different ecological dimensions respond to different social drivers.

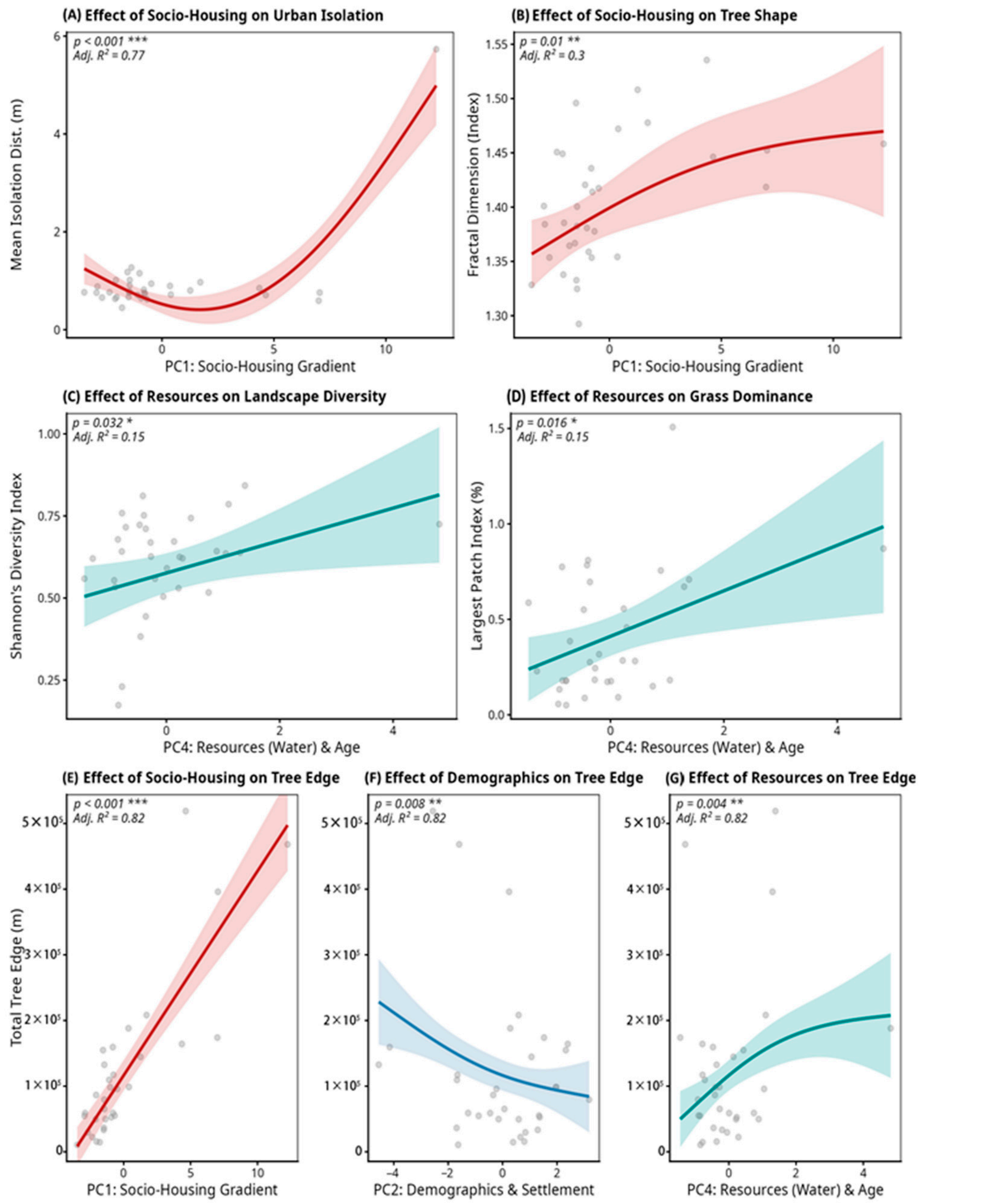

Figure 3. Significant associations between socioeconomic gradients and selected landscape metrics modeled using generalized additive models (GAMs). (**A**) Effect of the Socio-Housing Gradient (PC1) on Urban Isolation, measured as the mean Euclidean nearest-neighbor distance of the non-vegetated class. (**B**) Effect of the Socio-Housing Gradient (PC1) on Tree Shape, measured as the fractal dimension of tree patches. (**C**) Effect of the Resources and Age Gradient (PC4) on Landscape Diversity, measured by Shannon's Diversity Index (SHDI). **(D)** Effect of the Resources and Age Gradient (PC4) on Grass Dominance, measured by the Largest Patch Index (LPI) of the low-vegetation class. (**E**) Effect of the Socio-Housing Gradient (PC1) on Total Tree Edge. (**F**) Effect of the Demographics and Settlement Gradient (PC2) on Total Tree Edge. (**G**) Effect of the Resources and Age Gradient (PC4) on Total Tree Edge. In all panels, solid lines represent the fitted smooth terms, shaded areas indicate the 95% confidence intervals, and points represent observed values. Colors identify the specific socioeconomic drivers. Asterisks indicate significance levels: * $p < 0.05$, ** $p < 0.01$, *** $p < 0.001$.

3.6.1. Determinants of Urban Forest Structure

The most robust relationship was observed for the structural configuration of woody vegetation. The model for Total Tree Edge explained 82.3% of the deviance (R2 = 0.823, see Figure 3 and Table S4 of the Supplementary Material), demonstrating that the physical presence of tree boundaries is strongly determined by socioeconomic factors. Specifically, this metric exhibited significant responses to three distinct gradients (Figure 3E–G): the Socio-Housing Gradient (PC1) showed a strong positive association ($p < 0.001$), indicating that neighborhoods with consolidated housing infrastructure display a dramatic increase in tree edges. Furthermore, Demographic Structure (PC2) exhibited a significant relationship ($p = 0.008$), while Resource Access (PC4) displayed a positive effect ($p = 0.004$), reinforcing the role of basic infrastructure in maintaining arboreal structures. Additionally, the geometric complexity of these trees, measured by Fractal Dimension, was significantly driven by PC1 ($p = 0.009$, Figure 3B), suggesting that wealthier neighborhoods typically feature tree patches with more complex spatial shapes compared to the simpler patterns found in vulnerable areas.

3.6.2. Urban Isolation and Density

The spatial arrangement of the built environment (non-vegetated class) showed the strongest dependency on housing density. The model for Urban Isolation (ENN_MN.0) explained 76.5% of the deviance (R2 = 0.765) and was driven exclusively by PC1 ($p < 0.001$, Figure 3A). This confirms a direct negative relationship: as housing density and consolidation increase (high PC1), the physical isolation between built-up patches decreases drastically.

3.6.3. Influence of Resources on Diversity and Grass Cover

In contrast to the structural metrics of trees, landscape diversity and low vegetation (grass) were not driven by the main socio-housing gradient (PC1) but rather by the specific gradient of Resource Access and Aging (PC4). The model for Landscape Diversity (SHDI) explained 14.7% of the variance, with PC4 being the only significant predictor ($p = 0.032$, Figure 3C). Similarly, Grass Dominance was significantly associated with PC4 ($p = 0.016$, Figure 3D). These findings indicate that the overall heterogeneity of the green landscape and the maintenance of herbaceous cover are more sensitive to water availability and neighborhood age than to housing density or income levels per se. Other metrics, such as Urban Shape Complexity and Tree Dominance, did not show statistically significant relationships with the socioeconomic predictors.

3.7. Operationalization of Inclusive Strategies: GIPI-Based Prioritization, Robustness, Spatial Patterns, and Intervention Typology

Equity-oriented green infrastructure planning was operationalized by computing the Green Infrastructure Prioritization Index (GIPI) for 33 Neighborhood Units, integrating a normalized green deficit component (G_{def}) and a normalized social vulnerability component (V) with equal weights ($w_g = w_v = 0.5$). GIPI values were then mapped as a continuous surface (Figure 4A) and classified into terciles (Low/Medium/High) to support decision-ready prioritization (Figure 4B). Under the default weighting, GIPI ranged from 0.318 to 0.740 (median 0.528), and the tercile classification produced 11 units per class. Across terciles, high-priority units concentrated the combined burden of social vulnerability and green deficit (Table 3). Compared with Low-priority units, High-priority units displayed higher median vulnerability (0.752 vs. 0.518) and higher median green deficit (0.443 vs. 0.284). In parallel, High-priority units showed less favorable spatial structure for woody vegetation (trees and shrubs), characterized by lower dominance of the largest woody patch (LPI 3, median 0.244 vs. 0.551 in Low) and higher isolation/structural discontinuity signals (e.g., ENN_MN3, Table 3), consistent with reduced continuity of woody vegetation where vulnerability is greatest.

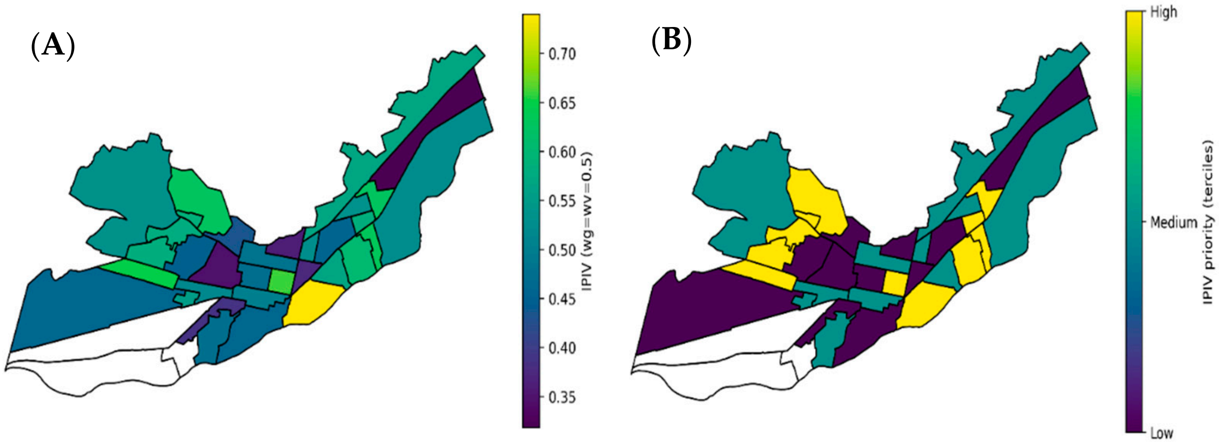

Figure 4. Equity-oriented green infrastructure prioritization (GIPI) across Neighborhood Units in Temuco. (**A**) Continuous spatial distribution of the GIPI, integrating woody vegetation deficit and socio-economic vulnerability. (**B**) Tercile-based priority classes (Low, Medium, and High) for operational targeting. Unfilled polygons indicate units excluded from the analytical dataset due to UAV operational restrictions associated with their proximity to the aerodrome/airport safety zone.

Table 3. GIPI stratification by priority class. Median and range of GIPI, vulnerability, and trees–shrubs landscape metrics across Low/Medium/High terciles.

Priority	*N*	GIPI (Median)	GIPI (Min–Max)	V (Median)	G_{def} (Median)	PROP_VEG (Median)	ENN_MN 3 (Median)	ED 3 (Median)	LPI 3 (Median)
High	11	0.625	0.581–0.740	0.752	0.443	0.202	5.098	792.097	0.244
Medium	11	0.528	0.474–0.567	0.621	0.443	0.198	5.756	726.290	0.229
Low	11	0.435	0.318–0.470	0.518	0.284	0.248	4.414	902.378	0.551

Spatially, the continuous GIPI map (Figure 4A) highlights a dominant hotspot (highest GIPI) and several additional high-value polygons, indicating that equity-relevant deficits are multinuclear rather than confined to a single contiguous area. The tercile map (Figure 4B) translates this gradient into an implementable targeting scheme, distinguishing a set of high-priority units suitable for first-phase intervention.

Sensitivity analyses varying the weight on green deficit (w_g) from 0.30 to 0.70 (step 0.05) indicated that prioritization is largely robust to plausible weighting choices. Of the 11 baseline High-priority units, 10 remained classified as High in ≥80% of weight settings (Table 4), supporting a stable set of priority targets under alternative "equity vs. biophysical deficit" trade-offs. One unit (Central) behaved as a borderline case (High frequency = 0.667), indicating that its class membership depends on the relative emphasis placed on V versus G_{def}; for such cases, interpretation should rely on the continuous GIPI gradient (Figure 4A) in addition to tercile membership.

To make explicit the combination underlying the GIPI, a V–G_{def} bivariate map was incorporated (Figure 5) that assigns Neighborhood Units to four decision-oriented quadrants. This visualization enables the rapid identification of areas where high social vulnerability co-occurs with pronounced green deficits (high V and high G_{def}), which largely correspond to the units classified as high priority by the GIPI (Figure 4). In addition, the bivariate map highlights borderline cases, such as units with high vulnerability but comparatively lower green deficit, or units with high green deficit in contexts of lower vulnerability. These patterns help interpret the differences observed under alternative weighting scenarios and strengthen the transparency, traceability, and robustness of the prioritization framework.

Table 4. High-priority units: robustness and dominant deficit type. Ranked High-tercile Neighborhood Units with GIPI components, deficit typology, and sensitivity-based robustness (High frequency, Robust High).

Neighborhood Unit	GIPI	V	G_{def}	Dominant Deficit	Robust High (≥80% Weight Settings)	High Frequency
San Antonio	0.740	1.000	0.480	Connectivity deficit	True	1.000
Central	0.660	0.320	1.000	Coverage deficit	False	0.667
Millaray	0.649	0.749	0.548	Connectivity deficit	True	1.000
Pomona	0.632	0.892	0.372	Coverage deficit	True	1.000
Vista Hermosa	0.626	0.867	0.385	Coverage deficit	True	1.000
Evaristo Marin	0.625	0.693	0.557	Coverage deficit	True	1.000
Santa Rosa	0.604	0.752	0.456	Connectivity deficit	True	1.000
Los Laureles	0.587	0.832	0.342	Coverage deficit	True	1.000
Ñielol	0.584	0.737	0.431	Coverage deficit	True	0.889
Igualdad y Trabajo	0.582	0.929	0.236	Connectivity deficit	True	0.889
Campos Deportivos	0.581	0.922	0.239	Mixed (coverage + connectivity)	True	1.000

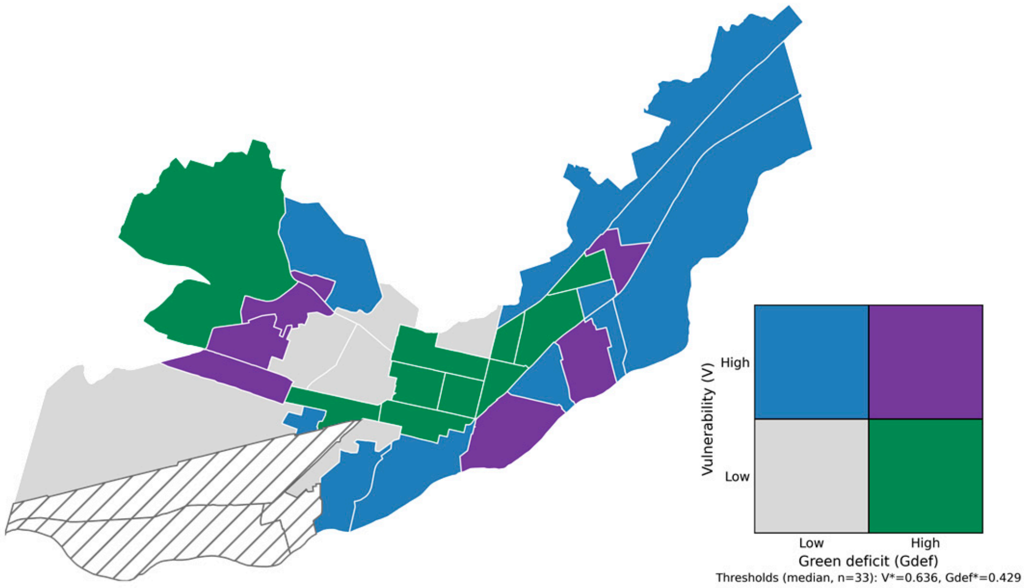

Figure 5. Bivariate map of social vulnerability (V) and green deficit (G_{def}) at the Neighborhood Unit scale, identifying areas where social vulnerability co-occurs with pronounced green deficits. Thresholds were defined using the sample median (n = 33), where V^* = 0.636 and G_{def}^* = 0.429. The asterisk denotes the cutoff value used to separate low and high classes in the bivariate classification. The hatched area indicates a sector excluded from the analysis due to UAV operational restrictions associated with its proximity to the aerodrome/airport safety zone.

Finally, to translate prioritization into implementable planning actions, each High-priority unit was assigned a dominant deficit type based on whether deficits were driven primarily by woody vegetation coverage (woody canopy and shrub scarcity), connectivity (woody patch isolation and discontinuity), or a mixed profile. This classification links recommended interventions directly to measurable outputs from the landscape analysis (Table 5). Among High-priority units, coverage deficits dominated in six units, connectivity deficits in four units, and one unit exhibited a mixed deficit profile, which supports a phased strategy that first expands canopy at key nodes and then strengthens structural linkage through linear greening.

Table 5. Intervention typology linked to measurable deficits (trees and shrubs). Decision-oriented intervention menu mapping coverage/connectivity deficit types to actionable strategies and monitoring indicators.

Deficit Type	Operational Meaning	Recommended Interventions	Monitoring Indicators (Repeatable)
Woody Vegetation coverage deficit	Scarcity of woody canopy/shrub layer (low woody vegetation contribution; low overall vegetated proportion)	Shade- and heat-mitigation greening: street-tree infill, canopy node planting, greening of schools/health facilities/public spaces, shrub–tree mixtures for rapid structure	PROP_VEG; SUP3/SUP_TOTAL; LPI 3
Woody Vegetation connectivity deficit	Woody patches are isolated/discontinuous (weak structural continuity)	Connectivity strengthening: continuous street-tree corridors, stepping-stone woody patches, linkage of canopy nodes, interventions along mobility/heat-exposure corridors	ENN_MN 3; ED 3; LPI 3
Mixed (coverage + connectivity)	Simultaneous scarcity and isolation of woody vegetation	Phased strategy: (1) increase woody canopy nodes, (2) connect nodes via linear greening/corridors; integrate maintenance and survival planning	PROP_VEG + ENN_MN 3 + ED 3 + LPI 3

4. Discussion

4.1. Socio-Spatial Inequities in Urban Vegetation Extend Beyond "How Much Green" to "How Green Is Arranged"

This study provides evidence that socio-spatial inequities in Temuco are expressed not only in the amount of vegetated cover but also in the spatial configuration of woody vegetation, a dimension increasingly recognized as critical for the delivery of ecosystem services and exposure-related benefits in cities. Landscape configuration modulates cooling intensity, with synthesis work showing that aggregation, shape complexity, and connectivity of urban green spaces can substantially influence thermal outcomes even when total green area is held constant [58]. Likewise, a growing body of evidence indicates that inequities in tree canopy and green exposure are pervasive and often patterned along socioeconomic gradients, with disadvantaged communities frequently experiencing lower canopy and reduced "green quality" [22,67].

Interpreting these results through this lens, the observed coupling between socioeconomic gradients and woody vegetation structure suggests that inequity in Temuco likely manifests as compound disadvantage: lower woody cover and weaker continuity can translate into reduced daily shade provision, diminished cooling along mobility corridors, and compromised habitat quality for urban biodiversity. This interpretation is coherent with current evidence that urban heat is persistent in built-up environments and that mitigation strategies should explicitly consider spatial pattern and placement of vegetation, not solely overall coverage [68,69].

4.2. Methodological Contribution: VHR OBIA Enables Policy-Relevant Separation of Woody Vegetation and Supports Equity Diagnostics

A key methodological contribution is the use of very high-resolution (VHR) imagery within an object-based image analysis (OBIA) framework to produce an operational separation of vegetation strata, enabling a specific focus on woody vegetation. OBIA approaches are widely used for urban vegetation mapping because they integrate spectral and spatial information, improving performance in heterogeneous urban mosaics compared with pixel-based methods [70]. This is consistent with recent reviews emphasizing that VHR data and object-based workflows are particularly appropriate where management and equity questions require fine-grain representation of vegetation form and distribution.

Beyond mapping, this analytical strategy advances toward inference by linking vegetation composition and configuration to socioeconomic gradients using flexible non-linear modeling. This aligns with a broader trend in urban environmental research that increasingly uses non-linear statistical learning and smoothers to detect thresholds and context-dependence in socio-ecological relationships [22,71]. In practical terms, the combination of VHR OBIA outputs with landscape metrics allows planners to move from coarse "green/no green" diagnostics to actionable understanding of where deficits are mainly coverage-related versus connectivity-related, which matter for different intervention portfolios.

4.3. From Diagnostics to Decision: GIPI Converts Remote-Sensing Outputs into Inclusive Planning Priorities and Is Robust to Normative Weighting Choices

From a planning perspective, the value of this framework lies not only in its capacity to detect fine-scale vegetation deficits, but also in its ability to interpret them through operational and policy-communicable benchmarks. In this study, the use of the World Health Organization-related accessibility criterion for public green space and the 3–30–300 guideline helped frame observed deficits as actionable planning gaps rather than as purely descriptive spatial patterns [72–74]. This is especially relevant in intermediate Latin American cities, where rapid urban expansion, heterogeneous urban fabrics, and persistent socio-spatial inequality often generate mismatches between social need and the distribution or structural quality of urban vegetation [5,7,75,76]. Recent regional evidence further underscores the heterogeneity and planning relevance of these dynamics by documenting substantial variability in the amount and spatial configuration of urban green space across Latin American cities, together with uneven provision associated with socioeconomic and built-environment conditions [5,75,76]. In this context, frameworks that combine fine-grained vegetation structure with explicit vulnerability lenses can help translate inequity mapping into more transparent and operational prioritization strategies [1,73,74].

A central contribution of the revised manuscript is the explicit translation of these remote-sensing and socio-spatial diagnostics into a decision-ready prioritization framework through the Green Infrastructure Prioritization Index (GIPI), which integrates standardized green deficit (G_{def}) and social vulnerability (V). Under equal weighting ($w_g = w_v = 0.5$), GIPI ranged from 0.318 to 0.740 (median = 0.528), and tercile-based classification produced 11 units per class (Table 4).

The continuous GIPI map (Figure 4A) and tercile prioritization map (Figure 4B) jointly indicate that equity-relevant deficits in Temuco are multinuclear rather than confined to a single contiguous zone. This spatial pattern is consistent with recent high-resolution assessments showing that compliance with 3–30–300 is often patchy within cities and that canopy shortfalls can persist even where some components of the rule are met [73,74].

Crucially, the prioritization is not an artifact of a single normative choice. Sensitivity analyses varying wg from 0.30 to 0.70 show that 10 of 11 baseline High-priority units remain High in at least 80% of weight settings (Table 4), which strengthens the policy credibility of the priority set. The borderline behavior of CENTRAL (Robust High = FALSE; High frequency = 0.667) should be interpreted as a transparent signal of classification sensitivity: its priority status depends on the relative emphasis placed on vulnerability versus green deficit, and therefore warrants interpretation using the continuous GIPI gradient (Figure 4A) alongside terciles. This practice is consistent with recommendations in equity-oriented urban forestry to make value judgments explicit and to distinguish robust from borderline targets when allocating scarce greening resources [71,77].

Although developed for Temuco, the outcomes of this study have broader relevance for other Chilean municipalities and intermediate Latin American cities facing similar combinations of rapid urban expansion, socio-spatial inequality, and uneven green infrastructure provision. The framework is potentially transferable because it is built on analytical components that can be adapted to different local contexts, including high-resolution vegetation mapping, neighborhood-scale socioeconomic indicators, and an explicit prioritization logic linking ecological deficits with social vulnerability. Its applicability, however, depends on the availability of spatially explicit socioeconomic data, comparable territorial units, and local calibration of planning benchmarks, weighting schemes, and intervention priorities. In this sense, rather than proposing a one-size-fits-all model, the study offers a flexible and decision-oriented workflow that can support context-sensitive urban greening strategies in other districts and municipalities across Chile and the wider region.

4.4. Intervention Implications: Deficit Typology Supports Targeted Design, but Implementation Must Incorporate Justice Safeguards to Prevent Displacement

To translate prioritization into implementable planning actions, each High-priority unit was classified by its dominant deficit profile, distinguishing woody vegetation coverage deficits, woody vegetation connectivity deficits, and mixed profiles, thereby linking recommendations directly to measurable outputs from the landscape analysis (Table 5). Among High-priority units, coverage deficits dominated in six units, connectivity deficits in four units, and one unit exhibited a mixed deficit profile. This distribution supports a phased strategy that expands canopy at key nodes first and then strengthens structural linkage through linear greening and corridor-like interventions, consistent with evidence that both vegetation type and configuration shape the magnitude and persistence of climate regulation benefits [58,69]. At the same time, high-impact environmental justice research cautions that greening initiatives can contribute to green gentrification when new or upgraded green amenities increase land values and attract displacement pressures in historically disinvested neighborhoods [16,78,79]. This risk has motivated the "just green enough" approach, which emphasizes co-design, prioritization of everyday benefits for current residents, and governance mechanisms that prevent displacement or exclusion [16,78]. Accordingly, while GIPI strengthens distributional justice by targeting areas where vulnerability and green deficit co-occur, implementation should be coupled with procedural safeguards (e.g., participatory design, transparent criteria, monitoring of distributive outcomes) to ensure that benefits accrue locally and equitably, as urged by recent urban forestry justice scholarship [71,79].

4.5. Positioning Temuco in the Broader Literature: Convergence with Global Findings and Added Value for Global South Equity Planning

Results from this study converge with global syntheses documenting that green and tree-related benefits are often unequally distributed and that disadvantaged groups may experience the strongest marginal health gains from improved green exposure, highlighting the equity relevance of prioritizing interventions in high-vulnerability areas [79,80]. They also resonate with emerging global analyses indicating widening disparities in exposure to urban greenspaces across regions, including patterns that disadvantage parts of the Global South [81].

The added value of this contribution lies in bridging three components that are still too often treated separately: (i) VHR mapping that differentiates woody vegetation structure, (ii) configuration-aware landscape metrics that capture fragmentation and continuity, and (iii) an equity-explicit prioritization index with robustness checks and an intervention typology. This "mapping-to-planning" pipeline responds directly to calls for practical measurement and implementation guidance around equity benchmarks such as 3–30–300, where recent work emphasizes that monitoring and operationalization remain key barriers to adoption [73,74].

4.6. Limitations and Future Directions

Several limitations delimit interpretation and point to a clear research agenda. First, the analysis is cross-sectional and cannot on its own establish causal pathways linking socioeconomic change, policy histories, and vegetation dynamics. Longitudinal VHR imagery and policy timeline reconstruction would strengthen causal inference and allow direct assessment of whether greening trajectories coincide with neighborhood change processes. Second, landscape metrics capture spatial pattern but are not direct measures of human exposure at street level (e.g., shade along walking networks) or of green quality (e.g., maintenance, safety, accessibility). Integrating network-based accessibility, street-level canopy indicators, and field audits would improve health- and equity-relevance and strengthen alignment with benchmarking frameworks [73,80]. Third, while GIPI offers transparency via sensitivity analyses, local implementation will benefit from additional scenario testing that explicitly evaluates different normative weightings and policy constraints (e.g., planting feasibility, infrastructure conflicts, irrigation limits), as highlighted by practice-oriented environmental justice work in urban forestry [58,71].

The evidence indicates that urban vegetation inequity in Temuco is simultaneously a problem of composition (woody versus non-woody vegetation), configuration (continuity and patch structure), and social vulnerability (who bears the deficit). By combining VHR OBIA mapping, configuration-aware metrics, and a robustness-tested prioritization index linked to an intervention typology, the study advances from diagnosis to implementable, equity-oriented action while remaining explicit about normative choices and attentive to the documented risk of unintended distributive consequences [16,82]

5. Conclusions

This study demonstrates how very high-resolution (VHR) UAV remote sensing can be translated into equity-oriented, decision-ready evidence for urban green infrastructure planning by integrating object-based vegetation mapping, landscape configuration metrics, socioeconomic gradients, and a robustness-tested prioritization index. The OBIA workflow captured pronounced intra-urban heterogeneity in land-cover composition and vegetation structure at the Neighborhood Unit scale, providing the spatial granularity required to identify where deficits are not only a function of total green area but also of how vegetation is distributed within neighborhoods.

A key finding is that inequities are strongly expressed in the spatial structure of woody vegetation. Configuration metrics revealed substantial contrasts in dominance, fragmentation, and isolation of woody patches among Neighborhood Units, indicating that the functional "quality" of green structure varies markedly within the city. This is planning-relevant because woody configuration is directly linked to the continuity of shade and the capacity for microclimate regulation, and therefore offers a more actionable diagnostic than area-only measures.

The socio-ecological modeling further shows that socioeconomic gradients relate to distinct ecological dimensions in non-linear yet interpretable ways. Dimensionality reduction in socioeconomic indicators yielded gradients consistent with differentiated urban processes (e.g., socio-housing consolidation and density, demographic–cultural structure, and resource access/aging), and GAM analyses indicated that woody-structure metrics are most strongly associated with the dominant socio-housing gradient, whereas other landscape attributes respond to different socioeconomic dimensions. Together, these results support the conclusion that urban green inequities in Temuco are multi-dimensional and cannot be reduced to a single socioeconomic proxy.

The Green Infrastructure Prioritization Index (GIPI) advances a "mapping-to-planning" pipeline by converting remote-sensing outputs into transparent, equity-explicit priorities. GIPI produced a ranked set of priority Neighborhood Units and tercile-based categories suitable for phased implementation, while sensitivity analyses demonstrated that the high-priority set is largely stable across plausible weighting choices and explicitly identified borderline cases where classification is weight-sensitive. By linking high-priority units to dominant deficit profiles (woody coverage deficits, woody connectivity deficits, or mixed conditions), the framework yields an implementable intervention typology with clear monitoring indicators, strengthening reproducibility and accountability. Overall, this study demonstrates that assessing urban green infrastructure through high-resolution spatial data and landscape configuration metrics provides a more nuanced understanding of environmental inequities than approaches based solely on green cover. By explicitly integrating biophysical patterns with socioeconomic gradients, this framework advances the translation of detailed diagnostics into decision-relevant planning insights. While the specific spatial outcomes are context-dependent, the proposed approach is transferable to other intermediate cities facing similar challenges. These findings highlight the need to move beyond purely descriptive assessments toward equity-oriented, evidence-based strategies for urban green infrastructure planning.

Although calibrated for Temuco, the proposed framework is potentially applicable to other Chilean municipalities and intermediate Latin American cities, provided that local socioeconomic indicators, spatial units, and planning benchmarks are appropriately adapted to the territorial context.

Supplementary Materials: The following supporting information can be downloaded at: https://www.mdpi.com/article/10.3390/land15040574/s1. Table S1: Confusion matrix for the OBIA-based classification of High Vegetation, Low Vegetation, and No Vegetation using 300 validation points, including Overall Accuracy (OA) and Kappa coefficient (κ); Table S2: Descriptive statistics of the 22 socioeconomic indicators used as input for the Principal Component Analysis (PCA) across the 33 Neighborhood Units of Temuco; Table S3: Descriptive statistics of the 23 landscape metrics characterizing the spatial configuration of urban vegetation and built-up areas; Table S4: Full statistical summary of the Generalized Additive Models (GAMs) fitted for the eight selected landscape metrics, including adjusted R^2, deviance explained, estimated degrees of freedom (edf), F-statistics, and *p*-values for each predictor; Figure S1: Heatmap showing the correlations between the 22 socioeconomic indicators and the four retained principal components (PC1–PC4); Figure S2: Correlation matrix of the 23 calculated landscape metrics, identifying the main redundancy clusters and the variables selected for subsequent modeling.

Author Contributions: Conceptualization, G.C., A.A. and C.D.B.; Methodology, C.M.-O., R.R.-R., G.C. and P.M.; Writing—original draft, G.C., A.A., C.D.B., P.M., F.D.L.B., R.V.-G., R.R.-R. and S.R.-P.; Writing—review and editing, G.C., A.A., C.D.B., P.M., F.D.L.B., R.V.-G., R.R.-R. and S.R.-P.; Funding acquisition, G.C. and A.A. All authors have read and agreed to the published version of the manuscript.

Funding: This research was funded by the National Doctoral Scholarship 21191900 (National Agency for Research and Development; ANID). The APC was funded by Universidad de La Frontera.

Data Availability Statement: Supplementary Materials provide complete replication resources that follow FAIR principles [83]. Raw very-high-resolution UAV imagery/orthomosaics may not be publicly shared due to privacy and regulatory constraints associated with fine-scale urban mapping, but can be made available from the corresponding author upon reasonable request for academic use.

Acknowledgments: We acknowledge additional support provided through the Internationalization Scholarship between Universidad de La Frontera and Universidad de Buenos Aires. We thank Universidad de La Frontera and Universidad de Buenos Aires for their invaluable support. A.A. gives thanks to Fondecyt grant 1211051. Partially funded by Universidad de La Frontera, PF24-0009. G.C. warmly acknowledges Martin, Alex, and Fernanda for their constant support and encouragement.

Conflicts of Interest: The authors declare no conflicts of interest.

References

1. Grabowski, Z.J.; McPhearson, T.; Pickett, S.T.A. Transforming US Urban Green Infrastructure Planning to Address Equity. *Landsc. Urban Plan.* **2023**, *229*, 104591. [CrossRef]
2. Rigolon, A.; Browning, M.H.E.M.; Lee, K.; Shin, S. Access to Urban Green Space in Cities of the Global South: A Systematic Literature Review. *Urban Sci.* **2018**, *2*, 67. [CrossRef]
3. Chen, B.; Wu, S.; Song, Y.; Webster, C.; Xu, B.; Gong, P. Contrasting Inequality in Human Exposure to Greenspace between Cities of Global North and Global South. *Nat. Commun.* **2022**, *13*, 4636. [CrossRef]
4. Li, Y.; Svenning, J.-C.; Zhou, W.; Zhu, K.; Abrams, J.F.; Lenton, T.M.; Ripple, W.J.; Yu, Z.; Teng, S.N.; Dunn, R.R.; et al. Green Spaces Provide Substantial but Unequal Urban Cooling Globally. *Nat. Commun.* **2024**, *15*, 7108. [CrossRef] [PubMed]
5. Bakhtsiyarava, M.; Moran, M.; Ju, Y.; Zhou, Y.; Rodriguez, D.A.; Dronova, I.; De Fatima Rodrigues Pereira De Pina, M.; De Matos, V.P.; Skaba, D.A. Potential Drivers of Urban Green Space Availability in Latin American Cities. *Nat. Cities* **2024**, *1*, 842–852. [CrossRef]
6. Venter, Z.S.; Shackleton, C.M.; Van Staden, F.; Selomane, O.; Masterson, V.A. Green Apartheid: Urban Green Infrastructure Remains Unequally Distributed across Income and Race Geographies in South Africa. *Landsc. Urban Plan.* **2020**, *203*, 103889. [CrossRef]
7. Flores, S.; Van Mechelen, C.; Vallejo, J.P.; Van Meerbeek, K. Trends and Status of Urban Green and Urban Green Research in Latin America. *Landsc. Urban Plan.* **2022**, *227*, 104536. [CrossRef]
8. Kundu, D.; Pandey, A.K. World Urbanisation: Trends and Patterns. In *Developing National Urban Policies*; Kundu, D., Sietchiping, R., Kinyanjui, M., Eds.; Springer Nature: Singapore, 2020; pp. 13–49.
9. Martinuzzi, A.; Blok, V.; Brem, A.; Stahl, B.; Schönherr, N. Responsible Research and Innovation in Industry—Challenges, Insights and Perspectives. *Sustainability* **2018**, *10*, 702. [CrossRef]
10. Cambridge University Press. *Intergovernmental Panel on Climate Change (IPCC) Climate Change 2022—Impacts, Adaptation and Vulnerability: Working Group II Contribution to the Sixth Assessment Report of the Intergovernmental Panel on Climate Change*, 1st ed.; Cambridge University Press: Cambridge, UK, 2023.
11. Bowler, D.E.; Buyung-Ali, L.; Knight, T.M.; Pullin, A.S. Urban Greening to Cool Towns and Cities: A Systematic Review of the Empirical Evidence. *Landsc. Urban Plan.* **2010**, *97*, 147–155. [CrossRef]
12. Armson, D.; Stringer, P.; Ennos, A.R. The Effect of Tree Shade and Grass on Surface and Globe Temperatures in an Urban Area. *Urban For. Urban Green.* **2012**, *11*, 245–255. [CrossRef]
13. Vujačić, D.; Stanovčić, T.; Gajić, T.; Aleksova, B.; Lukić, T. Advancing Urban Sustainability: Applying GIS Technologies to Assess SDG Indicators—A Case Study of Podgorica (Montenegro). *Open Geosci.* **2025**, *17*, 20250803. [CrossRef]
14. Han, L.; Lu, L.; Lu, J.; Liu, X.; Zhang, S.; Luo, K.; He, D.; Wang, P.; Guo, H.; Li, Q. Assessing Spatiotemporal Changes of SDG Indicators at the Neighborhood Level in Guilin, China: A Geospatial Big Data Approach. *Remote Sens.* **2022**, *14*, 4985. [CrossRef]
15. Zuniga-Teran, A.A.; Gerlak, A.K.; Elder, A.D.; Tam, A. The Unjust Distribution of Urban Green Infrastructure Is Just the Tip of the Iceberg: A Systematic Review of Place-Based Studies. *Environ. Sci. Policy* **2021**, *126*, 234–245. [CrossRef]
16. Anguelovski, I.; Connolly, J.J.T.; Cole, H.; Garcia-Lamarca, M.; Triguero-Mas, M.; Baró, F.; Martin, N.; Conesa, D.; Shokry, G.; Del Pulgar, C.P.; et al. Green Gentrification in European and North American Cities. *Nat. Commun.* **2022**, *13*, 3816. [CrossRef] [PubMed]
17. Norton, B.A.; Coutts, A.M.; Livesley, S.J.; Harris, R.J.; Hunter, A.M.; Williams, N.S.G. Planning for Cooler Cities: A Framework to Prioritise Green Infrastructure to Mitigate High Temperatures in Urban Landscapes. *Landsc. Urban Plan.* **2015**, *134*, 127–138. [CrossRef]
18. Meerow, S.; Newell, J.P. Spatial Planning for Multifunctional Green Infrastructure: Growing Resilience in Detroit. *Landsc. Urban Plan.* **2017**, *159*, 62–75. [CrossRef]
19. Nesbitt, L.; Meitner, M.J.; Girling, C.; Sheppard, S.R.J.; Lu, Y. Who Has Access to Urban Vegetation? A Spatial Analysis of Distributional Green Equity in 10 US Cities. *Landsc. Urban Plan.* **2019**, *181*, 51–79. [CrossRef]
20. Catalán, G.; Di Bella, C.; Meli, P.; De La Barrera, F.; Vargas-Gaete, R.; Reyes-Riveros, R.; Reyes-Packe, S.; Altamirano, A. Every Pixel You Take: Unlocking Urban Vegetation Insights Through High- and Very-High-Resolution Remote Sensing. *Urban Sci.* **2025**, *9*, 385. [CrossRef]
21. Shao, H.; Song, P.; Mu, B.; Tian, G.; Chen, Q.; He, R.; Kim, G. Assessing City-Scale Green Roof Development Potential Using Unmanned Aerial Vehicle (UAV) Imagery. *Urban For. Urban Green.* **2021**, *57*, 126954. [CrossRef]

22. Allegretto, G.; Kendal, D.; Flies, E.J. A Systematic Review of the Relationship between Urban Forest Quality and Socioeconomic Status or Race. *Urban For. Urban Green.* **2022**, *74*, 127664. [CrossRef]
23. Wood, S.N. *Generalized Additive Models: An Introduction with R*, 2nd ed.; Chapman and Hall/CRC: Boca Raton, FL, USA, 2017.
24. Clark, N.J.; Wells, K. Dynamic Generalised Additive Models (DGAMs) for Forecasting Discrete Ecological Time Series. *Methods Ecol. Evol.* **2023**, *14*, 771–784. [CrossRef]
25. Trinidad, S.; Brokamp, C.; Mor Huertas, A.; Beck, A.F.; Riley, C.L.; Rasnik, E.; Falcone, R.; Kotagal, M. Use Of Area-Based Socioeconomic Deprivation Indices: A Scoping Review and Qualitative Analysis: Study Examines Socioeconomic Deprivation Indices. *Health Aff.* **2022**, *41*, 1804–1811. [CrossRef] [PubMed]
26. Panczak, R.; Berlin, C.; Voorpostel, M.; Zwahlen, M.; Egger, M. The Swiss Neighbourhood Index of Socioeconomic Position: Update and Re-Validation. *Swiss Med. Wkly.* **2023**, *153*, 40028. [CrossRef] [PubMed]
27. Bolay, J.-C.; Rabinovich, A. Intermediate Cities in Latin America Risk and Opportunities of Coherent Urban Development. *Cities* **2004**, *21*, 407–421. [CrossRef]
28. Berdegué, J.A.; Carriazo, F.; Jara, B.; Modrego, F.; Soloaga, I. Cities, Territories, and Inclusive Growth: Unraveling Urban–Rural Linkages in Chile, Colombia, and Mexico. *World Dev.* **2015**, *73*, 56–71. [CrossRef]
29. Korah, A.; Wimberly, M.C. Smaller Cities Have Large Impacts on West Africa's Expanding Urban System. *Sustain. Cities Soc.* **2024**, *106*, 105381. [CrossRef]
30. Nugraha, E.; Wesely, J.; Ruszczyk, H.A.; De Villiers, I.; Zhao, Y. Overlooked Cities: Shifting the Gaze in Research and Practice in Global Urban Studies. *Cities* **2023**, *133*, 104044. [CrossRef]
31. Kendal, D.; Egerer, M.; Byrne, J.A.; Jones, P.J.; Marsh, P.; Threlfall, C.G.; Allegretto, G.; Kaplan, H.; Nguyen, H.K.D.; Pearson, S.; et al. City-Size Bias in Knowledge on the Effects of Urban Nature on People and Biodiversity. *Environ. Res. Lett.* **2020**, *15*, 124035. [CrossRef]
32. Sibaruddin, H.I.; Shafri, H.Z.M.; Pradhan, B.; Haron, N.A. Comparison of Pixel-Based and Object-Based Image Classification Techniques in Extracting Information from UAV Imagery Data. *IOP Conf. Ser. Earth Environ. Sci.* **2018**, *169*, 012098. [CrossRef]
33. Grebby, S.; Field, E.; Tansey, K. Evaluating the Use of an Object-Based Approach to Lithological Mapping in Vegetated Terrain. *Remote Sens.* **2016**, *8*, 843. [CrossRef]
34. Moskal, L.M.; Styers, D.M.; Halabisky, M. Monitoring Urban Tree Cover Using Object-Based Image Analysis and Public Domain Remotely Sensed Data. *Remote Sens.* **2011**, *3*, 2243–2262. [CrossRef]
35. Han, R.; Liu, P.; Wang, G.; Zhang, H.; Wu, X. Advantage of Combining OBIA and Classifier Ensemble Method for Very High-Resolution Satellite Imagery Classification. *J. Sens.* **2020**, *2020*, 8855509. [CrossRef]
36. Aguilar, M.A.; Aguilar, F.J.; García Lorca, A.; Guirado, E.; Betlej, M.; Cichon, P.; Nemmaoui, A.; Vallario, A.; Parente, C. Assessment of multiresolution segmentation for extracting greenhouses from worldview-2 imagery. *Int. Arch. Photogramm. Remote Sens. Spat. Inf. Sci.* **2016**, *XLI-B7*, 145–152. [CrossRef]
37. Elsebaei, M.; El-Naggar, A.M.; Abdel-maguid, R.K.; Elsebaei, M.A.; Ayaad, S.M. Identification of Optimal Segmentation Parameters for Extracting Buildings from Remote Sensing Images with Different Resolutions. *Benha J. Appl. Sci.* **2024**, *9*, 1–11. [CrossRef]
38. Lassiter, A.; Darbari, M. Assessing Alternative Methods for Unsupervised Segmentation of Urban Vegetation in Very High-Resolution Multispectral Aerial Imagery. *PLoS ONE* **2020**, *15*, e0230856. [CrossRef]
39. Zhang, P.; Lin, C.; Guo, S.; Zhang, W.; Fang, H.; Du, P. A Labor-Free Index-Guided Semantic Segmentation Approach for Urban Vegetation Mapping from High-Resolution True Color Imagery. *Int. J. Digit. Earth* **2023**, *16*, 1640–1660. [CrossRef]
40. Wang, W.; Cheng, Y.; Ren, Z.; He, J.; Zhao, Y.; Wang, J.; Zhang, W. A Novel Hybrid Method for Urban Green Space Segmentation from High-Resolution Remote Sensing Images. *Remote Sens.* **2023**, *15*, 5472. [CrossRef]
41. Cheng, Y.; Wang, W.; Ren, Z.; Zhao, Y.; Liao, Y.; Ge, Y.; Wang, J.; He, J.; Gu, Y.; Wang, Y.; et al. Multi-Scale Feature Fusion and Transformer Network for Urban Green Space Segmentation from High-Resolution Remote Sensing Images. *Int. J. Appl. Earth Obs. Geoinf.* **2023**, *124*, 103514. [CrossRef]
42. Yang, B.; Zhao, M.; Xing, Y.; Zeng, F.; Sun, Z. VEDAM: Urban Vegetation Extraction Based on Deep Attention Model from High-Resolution Satellite Images. *Electronics* **2023**, *12*, 1215. [CrossRef]
43. Rouse, J.W., Jr.; Haas, R.H.; Schell, J.A.; Deering, D.W. Monitoring Vegetation Systems in the Great Plains with Erts. In *NASA Special Publication*; NASA: Washington, DC, USA, 1974; Volume 351, p. 309.
44. Tucker, C.J. Red and Photographic Infrared Linear Combinations for Monitoring Vegetation. *Remote Sens. Environ.* **1979**, *8*, 127–150. [CrossRef]
45. Carlson, T.N.; Ripley, D.A. On the Relation between NDVI, Fractional Vegetation Cover, and Leaf Area Index. *Remote Sens. Environ.* **1997**, *62*, 241–252. [CrossRef]
46. Pettorelli, N.; Vik, J.O.; Mysterud, A.; Gaillard, J.-M.; Tucker, C.J.; Stenseth, N.C. Using the Satellite-Derived NDVI to Assess Ecological Responses to Environmental Change. *Trends Ecol. Evol.* **2005**, *20*, 503–510. [CrossRef]
47. Höfle, B.; Hollaus, M.; Hagenauer, J. Urban Vegetation Detection Using Radiometrically Calibrated Small-Footprint Full-Waveform Airborne LiDAR Data. *ISPRS J. Photogramm. Remote Sens.* **2012**, *67*, 134–147. [CrossRef]

48. Pu, R.; Landry, S. A Comparative Analysis of High Spatial Resolution IKONOS and WorldView-2 Imagery for Mapping Urban Tree Species. *Remote Sens. Environ.* **2012**, *124*, 516–533. [CrossRef]
49. Alonzo, M.; Bookhagen, B.; Roberts, D.A. Urban Tree Species Mapping Using Hyperspectral and Lidar Data Fusion. *Remote Sens. Environ.* **2014**, *148*, 70–83. [CrossRef]
50. Salehi, B.; Zhang, Y.; Zhong, M.; Dey, V. Object-Based Classification of Urban Areas Using VHR Imagery and Height Points Ancillary Data. *Remote Sens.* **2012**, *4*, 2256–2276. [CrossRef]
51. Wang, K.; Wang, T.; Liu, X. A Review: Individual Tree Species Classification Using Integrated Airborne LiDAR and Optical Imagery with a Focus on the Urban Environment. *Forests* **2018**, *10*, 1. [CrossRef]
52. Guo, J.; Huo, H. An Enhanced IT2FCM* Algorithm Integrating Spectral Indices and Spatial Information for Multi-Spectral Remote Sensing Image Clustering. *Remote Sens.* **2017**, *9*, 960. [CrossRef]
53. Zhao, Y.; Zhang, X.; Feng, W.; Xu, J. Deep Learning Classification by ResNet-18 Based on the Real Spectral Dataset from Multispectral Remote Sensing Images. *Remote Sens.* **2022**, *14*, 4883. [CrossRef]
54. McGarigal, K.; Marks, B.J. *FRAGSTATS: Spatial Pattern Analysis Program for Quantifying Landscape Structure*; U.S. Department of Agriculture, Forest Service, Pacific Northwest Research Station: Portland, OR, USA, 1995; p. PNW-GTR-351.
55. Zou, X.; Wang, C.; Que, X.; Ma, X.; Wang, Z.; Fu, Q.; Lai, Y.; Zhuang, X. Spatiotemporal Heterogeneous Responses of Ecosystem Services to Landscape Patterns in Urban–Suburban Areas. *Sustainability* **2024**, *16*, 3260. [CrossRef]
56. Benedetti, Y.; Morelli, F.; Svitok, M.; Santolini, R.; Kadlecová, P.; Cavalli, A.; Strollo, A.; Munafò, M. Identifying Landscape Characteristics That Maximize Ecosystem Services Provision. *Sustainability* **2024**, *16*, 9461. [CrossRef]
57. Ma, S.; Wang, L.; Wang, H.; Zhang, X.; Jiang, J. Spatial Heterogeneity of Ecosystem Services in Response to Landscape Patterns under the Grain for Green Program: A Case-study in Kaihua County, China. *Land Degrad. Dev.* **2022**, *33*, 1901–1916. [CrossRef]
58. Li, Y.; Ren, C.; Ho, J.Y.; Shi, Y. Landscape Metrics in Assessing How the Configuration of Urban Green Spaces Affects Their Cooling Effect: A Systematic Review of Empirical Studies. *Landsc. Urban Plan.* **2023**, *239*, 104842. [CrossRef]
59. Grafius, D.R.; Corstanje, R.; Harris, J.A. Linking Ecosystem Services, Urban Form and Green Space Configuration Using Multivariate Landscape Metric Analysis. *Landsc. Ecol.* **2018**, *33*, 557–573. [CrossRef] [PubMed]
60. Peroni, F.; Pristeri, G.; Codato, D.; Pappalardo, S.E.; De Marchi, M. Biotope Area Factor: An Ecological Urban Index to Geovisualize Soil Sealing in Padua, Italy. *Sustainability* **2019**, *12*, 150. [CrossRef]
61. Shpuza, E. The Shape and Size of Urban Blocks. *Environ. Plan. B Urban Anal. City Sci.* **2023**, *50*, 24–43. [CrossRef]
62. Aalipour, M.; Wu, N.; Fohrer, N.; Kianpoor Kalkhajeh, Y.; Jabbarian Amiri, B. Examining the Influence of Landscape Patch Shapes on River Water Quality. *Land* **2023**, *12*, 1011. [CrossRef]
63. Chen, Y.; Wang, J. Describing Urban Evolution with the Fractal Parameters Based on Area-Perimeter Allometry. *Discret. Dyn. Nat. Soc.* **2016**, *2016*, 4863907. [CrossRef]
64. Instituto Nacional de Estadísticas (INE), Chile. Dato Vecino. Available online: https://www.datovecino.gob.cl (accessed on 22 October 2022).
65. Michler, J.D.; Josephson, A.; Kilic, T.; Murray, S. Privacy Protection, Measurement Error, and the Integration of Remote Sensing and Socioeconomic Survey Data. *J. Dev. Econ.* **2022**, *158*, 102927. [CrossRef]
66. Zhu, Y.; Ling, G.H.T. Spatio-Temporal Changes and Driving Forces Analysis of Urban Open Spaces in Shanghai between 1980 and 2020: An Integrated Geospatial Approach. *Remote Sens.* **2024**, *16*, 1184. [CrossRef]
67. Gerrish, E.; Watkins, S.L. The Relationship between Urban Forests and Income: A Meta-Analysis. *Landsc. Urban Plan.* **2018**, *170*, 293–308. [CrossRef]
68. Li, D.; Wang, L.; Liao, W.; Sun, T.; Katul, G.; Bou-Zeid, E.; Maronga, B. Persistent Urban Heat. *Sci. Adv.* **2024**, *10*, eadj7398. [CrossRef] [PubMed]
69. Soltanifard, H.; Amani-Beni, M. The Cooling Effect of Urban Green Spaces as Nature-Based Solutions for Mitigating Urban Heat: Insights from a Decade-Long Systematic Review. *Clim. Risk Manag.* **2025**, *49*, 100731. [CrossRef]
70. Neyns, R.; Canters, F. Mapping of Urban Vegetation with High-Resolution Remote Sensing: A Review. *Remote Sens.* **2022**, *14*, 1031. [CrossRef]
71. Grant, A.; Millward, A.A.; Edge, S. Pursuit of Environmental Justice in Urban Forest Planning and Practice. *Front. Sustain. Cities* **2023**, *5*, 1233878. [CrossRef]
72. Przewoźna, P.; Inglot, A.; Mielewczyk, M.; Maczka, K.; Matczak, P. Accessibility to Urban Green Spaces: A Critical Review of WHO Recommendations in the Light of Tree-Covered Areas Assessment. *Ecol. Indic.* **2024**, *166*, 112548. [CrossRef]
73. Browning, M.H.E.M.; Locke, D.H.; Konijnendijk, C.; Labib, S.M.; Rigolon, A.; Yeager, R.; Bardhan, M.; Berland, A.; Dadvand, P.; Helbich, M.; et al. Measuring the 3-30-300 Rule to Help Cities Meet Nature Access Thresholds. *Sci. Total Environ.* **2024**, *907*, 167739. [CrossRef]
74. Croeser, T.; Sharma, R.; Weisser, W.W.; Bekessy, S.A. Acute Canopy Deficits in Global Cities Exposed by the 3-30-300 Benchmark for Urban Nature. *Nat. Commun.* **2024**, *15*, 9333. [CrossRef]

75. Dobbs, C.; Eleuterio, A.A.; Vásquez, A.; Cifuentes-Ibarra, M.; Da Silva, D.; Devisscher, T.; Baptista, M.D.; Hernández-Moreno, Á.; Meléndez-Ackerman, E.; Navarro, N.M. Are We Promoting Green Cities in Latin America and the Caribbean? Exploring the Patterns and Drivers of Change for Urban Vegetation. *Land Use Policy* **2023**, *134*, 106912. [CrossRef]
76. Ju, Y.; Moran, M.; Wang, X.; Avila-Palencia, I.; Cortinez-O'Ryan, A.; Moore, K.; Slovic, A.D.; Sarmiento, O.L.; Gouveia, N.; Caiaffa, W.T.; et al. Latin American Cities with Higher Socioeconomic Status Are Greening from a Lower Baseline: Evidence from the SALURBAL Project. *Environ. Res. Lett.* **2021**, *16*, 104052. [CrossRef]
77. Ponette-González, A.G.; Fry, M.; Hirschfeld, D.; Rose, J.; Elderbrock, E. Just Distribution of Tree Canopy? A Digital Approach to Tree Equity. *J. Am. Plan. Assoc.* **2026**, *92*, 125–133. [CrossRef]
78. Sax, D.L.; Nesbitt, L.; Quinton, J. Improvement, Not Displacement: A Framework for Urban Green Gentrification Research and Practice. *Environ. Sci. Policy* **2022**, *137*, 373–383. [CrossRef]
79. Rigolon, A. A Complex Landscape of Inequity in Access to Urban Parks: A Literature Review. *Landsc. Urban Plan.* **2016**, *153*, 160–169. [CrossRef]
80. Rigolon, A.; Browning, M.H.E.M.; McAnirlin, O.; Yoon, H.V. Green Space and Health Equity: A Systematic Review on the Potential of Green Space to Reduce Health Disparities. *Int. J. Environ. Res. Public Health* **2021**, *18*, 2563. [CrossRef]
81. Leng, S.; Sun, R.; Yang, X.; Chen, L. Global Inequities in Population Exposure to Urban Greenspaces Increased amidst Tree and Nontree Vegetation Cover Expansion. *Commun. Earth Environ.* **2023**, *4*, 464. [CrossRef]
82. Konijnendijk, C.C. Evidence-Based Guidelines for Greener, Healthier, More Resilient Neighbourhoods: Introducing the 3–30–300 Rule. *J. For. Res.* **2023**, *34*, 821–830. [CrossRef]
83. Wilkinson, M.D.; Dumontier, M.; Aalbersberg, I.J.J.; Appleton, G.; Axton, M.; Baak, A.; Blomberg, N.; Boiten, J.-W.; Da Silva Santos, L.B.; Bourne, P.E.; et al. The FAIR Guiding Principles for Scientific Data Management and Stewardship. *Sci. Data* **2016**, *3*, 160018. [CrossRef]